Journal of Crystal Growth 312 (2010) 3209–3213

Contents lists available at ScienceDirect

Journal of Crystal Growth

journal homepage: www.elsevier.com/locate/jcrysgro

Growth and optical properties of high-density InN nanodots

W.C. Ke [a,*], S.J. Lee [a], C.Y. Kao [a], W.K. Chen [b], W.C. Chou [b], M.C. Lee [b], W.H. Chang [b], W.J. Lin [c], Y.C. Cheng [c], T.C. Lee [c], J.C. Lin [c]

[a] Department of Mechanical Engineering, Yuan Ze University, Chung-Li 320, Taiwan, ROC
[b] Department of Electrophysics, National Chiao Tung University, Hsinchu 300, Taiwan, ROC
[c] Chung-Shan Institute of Science and Technology, Tao-Yuan 325, Taiwan, ROC

ARTICLE INFO

Article history:
Received 23 February 2010
Received in revised form
19 July 2010
Accepted 21 July 2010
Communicated by H. Fujioka
Available online 27 July 2010

Keywords:
A1. Nanostructures
A3. Metal–organic chemical vapor deposition
B1. InN
B2. Semiconducting indium compounds

ABSTRACT

High density InN/GaN nanodots were grown by pulsed mode (PM) metal–organic chemical vapor deposition (MOCVD). InN nanodots density of up to $\sim 5 \times 10^{10}\,cm^{-2}$ at a growth temperature of 550 °C was achieved. The high diffusion activation energy of 2.65 eV due to high NH_3 flow rate generated more reactive nitrogen adatoms on the growth surface, and is believed to be the main reason for the growth of high density InN nanodots. In addition, an anomalous temperature dependence of the PL peak energy was observed for high density InN nanodots. The high carrier concentration, due to high In vacancy (V_{In}) in the InN nanodots, thermally agitated to the conduction band. As the measurement temperature increased, the increase of Fermi energy resulted in blue-shifted PL peak energy. From the Arrhenius plot of integrated PL intensity, the thermal activation energy for the PM grown InN nanodots was estimated to be $E_a \sim 51$ meV, indicating strong localization of carriers in the high density InN nanodots.

1. Introduction

Since the InN band gap energy was revised to ~0.7 eV [1–3], this discovery has provided opportunities for further applications of III-nitride based optoelectronic devices. Recently there has been substantial interest in InGaN as a thin-film solar cells material because of its wide tunable energy band gap, which covers almost the entire solar spectrum. However, to date there are only a few reports on InGaN based solar cells due to some issues (phase separation, doping issue, poor quality material, etc.), which are difficult to overcome in the commercial MOCVD system [4–6]. In the past couple of years, the use of nanostructures in solar cells has offered the potential for a higher level of efficiency using physical concepts. For example, the benefit of multiple exciton generation (MEG) has been demonstrated in colloidal suspensions of PbSe, PbS, PbTe, CdSe, and GaAs quantum dots (QDs) [7–9]. A maximum theoretical efficiency of 42% has been predicted for single-junction devices employing MEG-active absorbers.

Nanostructured solar cells must include structures that increase absorption, which will increase the nanostructure volume. At the same time the devices must be kept thin enough to allow them to be carried around. Thus, there is an urgent need to develop a growth technique for high density QDs. High density of InN QDs was reported by Ruffenach et al. [10], who used argon as a carrier gas to achieve high density InN QDs. In our previous reports, a flow rate modulation epitaxy (FME) technique was established to grow InN nanodots of high optical quality on GaN films [11–13]. However, the density of InN nanodots grown by the FME technique is very low (i.e. $\sim 1 \times 10^9\,cm^{-3}$ at growth temperature of 550 °C).

Thus, this paper presents a method that is feasible for preparing high density InN nanodots on a GaN surface. Preliminary results indicate that by alternating the source precursor method, the so-called pulsed mode (PM) during the MOVPE epitaxial growth, high density InN nanodots could be achieved on a GaN epilayer. This method has been proven to be a simple yet effective way for preparing QDs structures in the InN material system and may have the potential to be used in the fabrication of infrared InN-based solar cells, light-emitting diodes, laser diodes, and detector devices. In addition, result of the anomalous temperature dependence of optical emission in high density InN nanodots was of great interest and was investigated as well.

2. Experimental details

The InN nanodots were grown on GaN/sapphire (0 0 0 1) at a temperature varying between 550 and 750 °C by the PM method using trimethylgallium (TMGa), trimethylindium (TMIn), and

* Corresponding author.
E-mail address: wcke@saturn.yzu.edu.tw (W.C. Ke).

0022-0248/$ - see front matter © 2010 Elsevier B.V. All rights reserved.
doi:10.1016/j.jcrysgro.2010.07.044

ammonia (NH_3) as the source materials. The gas flow sequence for the PM method basically consists of four steps: 20 s TMIn+NH_3 growth step, 20 s NH_3 source step with 10 s purge steps in between. During the growth step, the mole flow rates of TMIn and NH_3 are 1.53×10^1 and 4.46×10^5 μmole/min, respectively. It is worth noting that during the 20 s NH_3 source step, an amount of NH_3 (8.04×10^5 μmole/min) is introduced intentionally to achieve high density InN nanodots. The NH_3 flow rate in the TMIn+NH_3 growth step and in the NH_3 source step differs from the early report of the FME technique. In the FME method, the NH_3 flow rate in the TMIn+NH_3 growth step was low in order to obtain high optical quality InN nanodots. In the present study, the InN nanodots were also grown by the conventional mode (CM) method, in which the TMIn and NH_3 flow rates are kept constant at 1.53×10^1 and 4.46×10^5 μmole/min, respectively. The total growth time for the InN nanodots was 2 min, which is equal to the total time of six cycles of growth steps in the PM method. An NT-MDT Solver HV atomic force microscopy (AFM) system was used to perform the morphology measurement. Photoluminescence (PL) measurements were performed using the 488 nm line of an argon-ion laser as an excitation source. The PL signals were analyzed by a 0.5 m monochromator and detected by a cooled InGaAs photodiode with a cut-off wavelength at 2.05 μm.

3. Results and discussion

In order to understand the growth mechanism of the high density InN nanodots grown by the PM method, we performed a series experiment that changed the growth temperature from 550 to 750 °C. The quantitative structural properties of the InN nanodots are summarized in Table 1. The AFM images of the InN nanodots grown by these two growth methods are shown in Fig. 1. The InN nanodots grown at a higher temperature (>700 °C) show much larger deviations in their heights/diameters due to the bimodal size distribution. Thus, we only count the InN nanodots that are grown at a lower temperature (<650 °C). In addition to the average height and diameter of the InN nanodots, their density was estimated by calculating the number of nanodots islands with an area of 100 μm^2 in the AFM images. The InN nanodots density as a function of the reciprocal temperature is shown in Fig. 2. As anticipated, density of the nanodots depends greatly on substrate temperature. There are two distinct regions in our dots density curve, and the diving point is a temperature of ~700 °C for the PM and CM methods. As can be seen in Fig. 2, the dot density is gradually reduced from 5×10^{10} to 5.1×10^8 cm^{-2} as temperature is increased from 550 to 700 °C. The dot density then drops sharply with the further increase in temperature and eventually become zero, i.e. there is no dots growth, as the substrate temperature increases beyond 750 °C. For a growth temperature higher than 700 °C, dot density drops drastically and bimodal dot size distribution becomes evident. This is caused mainly by the coarsening of the dots as can be observed in Fig. 1(c) and (f). The coarsening of the dots was due to the need of the system to reduce the boundary of free energy by transforming small dots into larger ones. This process involves both migrations of adatoms across terraces and evaporation of atoms from dots. Consequently the dots density becomes a much steeper function of temperature.

Table 1
Average height and diameter of the InN nanodots grown by the PM and CM methods at temperatures ranging from 550 to 650 °C.

Sample (°C)	PM		CM	
	Height (nm)	Diameter (nm)	Height (nm)	Diameter (nm)
550	9 ± 0.9	75 ± 6	13 ± 1.1	102 ± 8
600	19 ± 1.6	125 ± 9	30 ± 4.0	184 ± 12
650	32 ± 3.8	238 ± 16	32.5 ± 4.2	220 ± 18

There are many processes involved in determining the density of the nanodots, such as nucleation barriers, temperature-dependent adatom attachment at existing islands, competing thermal dissociation, and others. With reference to the island nucleation mechanism proposed by Robinson and Robins [14], dot density at low temperature is governed by diffusion capability of the adatom. The respective characteristic equations are

$$N_s \propto N_{0L}\exp(E_d/3kT)$$

where N_s is the dot density and N_{0L} the pre-exponential parameter. The E_d activation energies are 2.65 and 1.25 eV for InN nanodots growth by PM and CM method, respectively. Because of the abundant supply of NH_3 (8.04×10^5 μmole/min) in the NH_3 source step, there is a large amount of nitrogen adatoms on the growing surface. It is believed that the higher activation energy in the PM method was due to the higher collision probability of the In adatoms with the high density of nitrogen adatoms on the GaN surface. Thus, high density InN nanodots is readily achieved by the PM method. In addition, Robinson's nucleation mechanism at high temperatures is determined predominately by re-evaporation rate of adatoms and hence binding energy of the adatom to the adsorbed site. However, the growth mechanism in the high growth temperature region (i.e. >650 °C) is very complex. In the competing mechanisms, for example, dissociation of InN nanodots, absorption and desorption of In adatom, coarsening InN nanodots, etc. must be considered simultaneously. Therefore, the growth mechanism at high temperature cannot be explained only by Robinson's model.

The growth efficiency of these two kinds of growth methods is shown in the inset of Fig. 2. The growth efficiency is defined by the InN nanodots volume divided by the mole flow rate of TMIn. Each InN nanodots volume was estimated using the dome structure. The volume of the nanodots was calculated by taking the volume of a single nanodot and multiplying it by the nanodot density for a 1 cm^2 area. For example, the total volume of nanodots was 1.47×10^{15} and 6.48×10^{14} nm^3, respectively, using the PM and CM method at 600 °C for a 1 cm^2 area. It must be noted that the growth efficiency curves show a maximum value at the growth temperature of 600 °C. It is known that NH_3 cracking efficiency increases with the increase in growth temperature. Thus, the increase of the growth efficiency the increase in growth temperature from 550 to 600 °C was believed to be relative to the increase in NH_3 cracking efficiency. However, the growth efficiency decreased with increase in growth temperature from 600 to 700 °C. This is evident from the increase in dissociation of the InN nanodots. In addition, growth efficiency for the PM method was about twice as large as that of the CM method. The higher growth efficiency for the PM method was believed to be due to the higher concentration of nitrogen atom participating in the growth of InN nanodots.

The 17 K PL spectra of the InN nanodots grown by the CM and PM methods at various growth temperatures of 600, 650, and 700 °C are shown in Fig. 3(a) and (b), respectively. It should be noted that these samples for PL measurement were without any GaN capping layer. The only noise signals observed in the PL spectra were for the InN nanodots grown at 550 °C. In addition, the emission energy and the full width at half maximum (FWHM) of the PL spectra for the InN nanodots, whether CM or PM methods, show an increasing trend when the temperature decreases from 700 to 600 °C. The 17 K PL spectra of the InN nanodots grown by the CM and PM methods are shown in Fig. 3(a) and (b), respectively. It should be noted that these

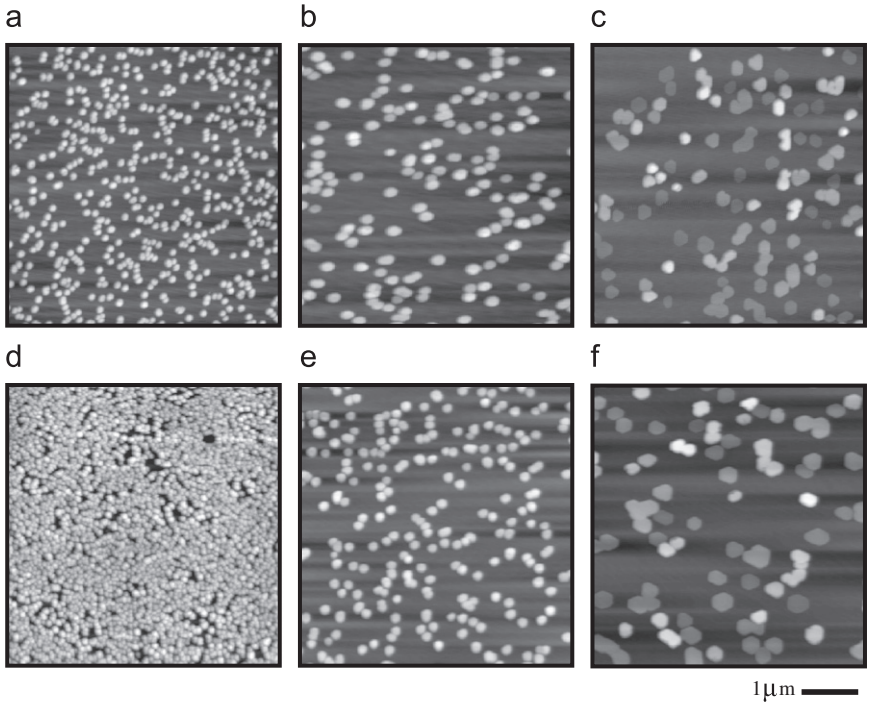

Fig. 1. AFM image of InN nanodots grown by the CM method at (a) 600 °C, (b) 650 °C, and (c) 700 °C. By the PM method at (d) 600 °C, (e) 650 °C, and (f) 700 °C.

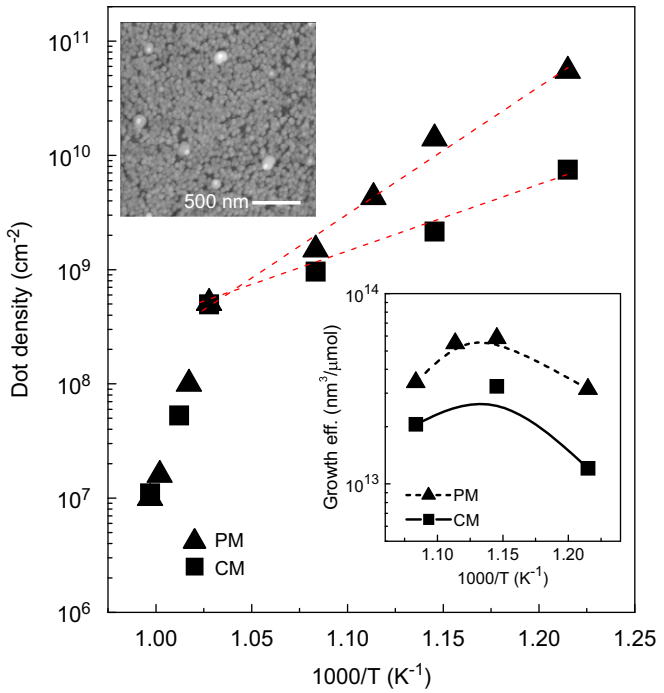

Fig. 2. InN nanodots density as function of 1000/*T*. The inset shows growth efficiency of the InN nanodots as a function of 1000/*T* for the CM and PM methods. The inset also shows the AFM image of the InN nanodots grown by the PM method at 550 °C.

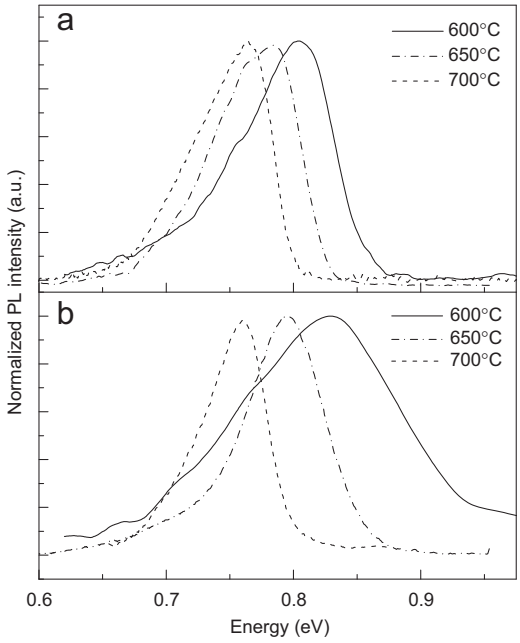

Fig. 3. The 17 K PL spectra of the InN nanodots grown by the CM and PM growth methods at various growth temperatures of 600, 650, and 700 °C. (a) CM and (b) PM.

samples for PL measurement were grown at 600 °C without any GaN capping layer. After considering the PL signal intensity and the density of the InN nanodots, we selected the 600 °C growth of the InN nanodots samples to represent the optical properties of the high density InN nanodots. The PL spectrum for the InN nanodots grown by the CM method at 600 °C shows a peak energy at 0.8 eV, with full width at half maximum (FWHM) of 87 meV. However, for the InN nanodots grown by the PM method at 600 °C, the PL peak energy was observed at 0.82 eV with FWHM of 143 meV. This emission energy of InN nanodots is higher than the reported band gap energy of 0.69 eV [15], indicating a strong Burstein–Moss effect due to the presence of high electron concentration in the InN nanodots. Since the dot size is still too large to produce a pronounced quantum size effect, any differences in the peak energy between two samples are due mainly to variations of electron concentration in the InN nanodots. In addition, Fu et al. [16] provide a convenient

formula to determine free-electron concentration in InN films by PL measurement. The relationship between FWHM and free-electron concentration can be well described by the empirical formula [17,18]. The free electron concentration was estimated as $\sim 7\times10^{18}$ and $\sim 2\times10^{19}\,cm^{-3}$, respectively, for the CM and PM growth of InN nanodots.

To further investigate the optical properties of the high density InN nanodots, this study conducted temperature-dependent PL measurements, which were then compared with InN nanodots grown by the CM method. The measured PL peak energies, using the two methods of InN nanodots as a function of temperature, are shown in Fig. 4(a). The PL signals could be observed clearly only for the temperature measurement below 170 K. It was found that the measured PL peak energy was less sensitive to temperature for the InN nanodots grown by the CM method. On the other hand we found that the PL peak energy increased with increase in temperature. A similar anomalous temperature dependence of optical emission was also reported for the porous Si and amorphous silicon quantum dots (a-Si QDs) [19,20]. Zheng et al. [19] indicated that the phonon spectrum depends on periodicity of the crystal lattice or microstructure. The average distance between pores or the pore density for porous Si was found to be the main reason for causing the anomalous peak energy shift in the PL spectrum.

The phonon-assisted Auger recombination rate plays an important role in samples with high carrier injection or high doping levels. According to Haug [21], the degenerating effect of a carrier in phonon-assisted Auger recombination remains mild until a carrier density of 10^{20} carriers/cm^3 is exceeded. The single type of vacancies in InN was identified as In vacancies or vacancy complexes containing V_{In} [22,23]. This In vacancy concentration was found to be correlated with free electron density and could possibly be an electron compensation defect [22]. If our case was phonon-assisted Auger recombination, then the V_{In} concentration would be higher than $10^{19}\,cm^{-3}$. In addition, there were no integrated PL intensity increases when temperature increased, something that is typically the case in a-Si QDs.

Several other effects were reported to explain the anomalous temperature dependence of optical emission, such as combination of the successive filling of localized states [24] and/or band tail states [25] in addition to Coulomb screening of the piezoelectric electric field [26] by thermally released or photo-generated carriers. In the present study it is our understanding that the anomalous temperature dependence of optical emission is a result of nitrogen rich stoichiometry, producing high densities of In vacancies, which act as free electrons in this particular type of sample. Cimalla et al. [27] reported that the high surface electron concentration generated by high surface density of state ($2-4\times10^{13}\,cm^{-2}$) was due to the high ratio of surface area to bulk volume of nanodots. Recently, Swartz et al. [28]. found that the surface electrons have a tendency to substantially increase when the temperature increases from 25 to 250 K. Thus, when the measured temperature increases, the number of trapped surface electrons that become thermally agitated to the conduction band increase substantially. This of course results in an increase of Fermi energy and subsequently a higher measured temperature for the blue-shifted PL energy of the emitted photons.

The carrier localization effect of the InN nanodots was further investigated using reduced thermal quenching of PL from the nanodots. Fig. 4(b) shows an Arrhenius plot of the integrated PL intensity for the InN nanodots grown by the PM and CM methods. It clearly shows reduced thermal quenching of PL from the InN nanodots. The thermal activation energy for the PM grown InN nanodots was estimated to be $E_a\sim51$ meV, which is significantly larger than the value $E_a\sim35$ meV for the CM grown InN nanodots, indicating stronger localization of carriers in the PM growth InN nanodots. This also suggests that the PL-quenching behaviors can be mitigated in small size nanodots, because of the stronger localization effect.

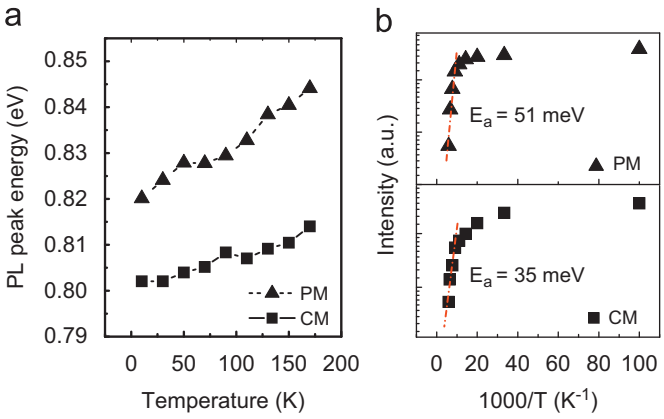

Fig. 4. (a) Temperature dependence of the PL peak energy and (b) Arrhenius plots of the integrated PL intensities for the CM and PM growth methods of InN nanodots.

4. Conclusions

High density InN/GaN nanodots ($\sim5\times10^{10}\,cm^{-2}$) were achieved by the PM MOCVD growth technique at a temperature of 550 °C. The high density InN nanodots were achieved mainly as a result of the high NH_3 flow rate in the NH_3 source step, resulting in a high density of nitrogen adatoms on the growing surface, and forming a diffusion barrier in the next growth step of the PM growth method. The higher PL peak energy and FWHM indicate that the free carrier concentration is higher for InN nanodots grown by the PM method. It is believed that the high carrier concentration due to the high In vacancy (V_{In}) in the InN nanodots is the main reason causing an anomalous temperature dependence of the PL peak energy for high density InN nanodots. In addition, the higher thermal activation energy of the InN nanodots indicates a stronger localization of carriers in the PM grown InN nanodots.

Acknowledgements

The authors gratefully acknowledge the financial support from the National Science Council of Taiwan, ROC, under Contract nos. NSC-98-2112-M155-001-MY3.

References

[1] V.Yu. Davydov, A.A. Klochikhin, R.P. Seisyan, V.V. Emtsev, S.V. Ivanov, F. Bechstedt, J. Furthmüller, H. Harima, A.V. Mudryi, J. Aderhold, O. Semchinova, J. Graul, Phys. Status Solidi B 229 (2002) R1.
[2] J. Wu, W. Walukiewicz, K.M. Yu, J.W. Ager III, E.E. Haller, H. Lu, W.J. Schaff, Y. Saito, Y. Nanishi, Appl. Phys. Lett. 80 (2002) 3967.
[3] T. Matsuoka, H. Okamoto, M. Nakao, H. Harima, E. Kurimoto, Appl. Phys. Lett. 81 (2002) 1246.
[4] O. Jani, I. Ferguson, C. Honsberg, S. Kurtz, Appl. Phys. Lett. 91 (2007) 132117.
[5] C.J. Neufeld, N.G. Toledo, S.C. Cruz, M. Iza, S.P. DenBaars, U.K. Mishra, Appl. Phys. Lett. 93 (2007) 143502.
[6] R. Dahal, B. Pantha, J. Li, J.Y. Lin, H.X. Jiang, Appl. Phys. Lett. 94 (2009) 063505.
[7] R.D. Schaller, V.I. Klimov, Phys. Rev. Lett. 92 (2004) 186601.
[8] G. Wei, S.R. Forrest, Nano Lett. 7 (2007) 218.
[9] S.M. Hubbard, C.D. Cress, C.G. Bailey, R.P. Raffaelle, S.G. Bailey, D.M. Wilt, Appl. Phys. Lett. 92 (2008) 123512.
[10] S. Ruffenach, O. Briot, M. Moret, B. Gil, Appl. Phys. Lett. 90 (2007) 153102.
[11] W.C. Ke, C.P. Fu, C.Y. Chen, L. Lee, C.S. Ku, W.C. Chou, W.-H. Chang, M.C. Lee, W.K. Chen, W.J. Lin, Y.C. Cheng, Appl. Phys. Lett. 88 (2006) 191913.

[12] W.C. Ke, L. Lee, C.Y. Chen, W.C. Tsai, W.-H. Chang, W.C. Chou, M.C. Lee, W.K. Chen, W.J. Lin, Y.C. Cheng, Appl. Phys. Lett. 89 (2006) 263117.
[13] W.H. Chang, W.C. Ke, S.H. Yu, L. Lee, C.Y. Chen, W.C. Tsai, H. Lin, W.C. Chou, M.C. Lee, W.K. Chen, J. Appl. Phys. Lett. 103 (2008) 104306.
[14] V.N.E. Robinson, J.L. Robins, Thin Solid Films 20 (1974) 155.
[15] F. Chen, A.N. Cartwright, H. Lu, W.J. Schaff, J. Cryst. Growth 269 (2004) 10.
[16] S.P. Fu, T.T. Chen, Y.F. Chen, Semicond. Sci. Technol. 21 (2006) 244.
[17] R.M. Sieg, S.A. Ringel, J. Appl. Phys. 80 (1996) 448.
[18] H.Q. Zheng, K. Radahakrishnan, S.F. Yoon, G.I. Ng, J. Appl. Phys. 87 (2000) 7988.
[19] X.L. Zheng, W. Wang, H.C. Chen, Appl. Phys. Lett. 60 (1992) 986.
[20] H.S. Kwack, Y. Sun, Y.H. Cho, N.M. Park, S.J. Park, Appl. Phys. Lett. 83 (2003) 2901.
[21] A. Huag, J. Phys. C 16 (1983) 4159.
[22] A. Laakso, J. Oila, A. Kemppinen, K. Saarinen, W. Egger, L. Liszkay, P. Sperr, H. Lu, W.J. Schaff, J. Cryst. Growth 269 (2004) 41.
[23] J. Oila, A. Kemppinen, A. Laakso, K. Saarinen, W. Egger, L. Liszkay, P. Sperr, H. Lu, W.J. Schaff, Appl. Phys. Lett. 84 (2004) 1486.
[24] P.G. Eliseev, P. Perlin, J. Lee, M. Osinski, Appl. Phys. Lett. 71 (1997) 569.
[25] P. Perlin, V. Iota, B.A. Weinstein, P. Wisniewski, T. Suski, P.G. Eliseev, M. Osinski, Appl. Phys. Lett. 70 (1997) 2993.
[26] H. Schömig, S. Halm, A. Forchel, G. Bacher, J. Off, F. Scholz, Phys. Rev. Lett. 92 (2004) 106802.
[27] V. Cimalla, V. Lebedev, F.M. Morales, R. Goldhahn, O. Ambacher, Appl. Phys. Lett. 89 (2006) 172109.
[28] C.H. Swartz, R.P. Tompkins, N.C. Giles, T.H. Myers, H. Lu, W.J. Schaff, L.F. Eastman, J. Cryst. Growth 269 (2004) 29.